Earth and Planetary Science Letters 302 (2011) 349–358

Contents lists available at ScienceDirect

Earth and Planetary Science Letters

journal homepage: www.elsevier.com/locate/epsl

Rapid cooling rates at an active mid-ocean ridge from zircon thermochronology

Axel K. Schmitt [a,*], Michael R. Perfit [b], Kenneth H. Rubin [c], Daniel F. Stockli [d], Matthew C. Smith [b], Laurie A. Cotsonika [b], Georg F. Zellmer [c,e], W. Ian Ridley [f], Oscar M. Lovera [a]

[a] Department of Earth and Space Sciences, University of California Los Angeles, 595 Charles Young Dr. E, Los Angeles, CA 90095, USA
[b] Department of Geological Sciences, University of Florida, Gainesville, Box 112120, FL 32611, USA
[c] Department of Geology and Geophysics SOEST, University of Hawaii, 1680 East West Rd, Honolulu, HI 96822, USA
[d] Department of Geology, University of Kansas, 120 Lindley Hall, 1475 Jayhawk Boulevard, Lawrence, KS 66045-7613, USA
[e] Institute of Earth Sciences Academia Sinica, 128 Academia Road, Sec. 2, Nankang, Taipei 11529, Taiwan, ROC
[f] U.S. Geological Survey, Central Region Mineral Resources Team, Box 25046, MS-973, Denver Federal Center, Denver, CO 80225, USA

ARTICLE INFO

Article history:
Received 15 September 2010
Received in revised form 6 December 2010
Accepted 8 December 2010
Available online 8 January 2011

Editor: R.W. Carlson

Keywords:
uranium series
(U–Th)/He dating
axial magma chamber
fractional crystallization
mid-ocean ridge volcanism

ABSTRACT

Oceanic spreading ridges are Earth's most productive crust generating environment, but mechanisms and rates of crustal accretion and heat loss are debated. Existing observations on cooling rates are ambiguous regarding the prevalence of conductive vs. convective cooling of lower oceanic crust. Here, we report the discovery and dating of zircon in mid-ocean ridge dacite lavas that constrain magmatic differentiation and cooling rates at an active spreading center. Dacitic lavas erupted on the southern Cleft segment of the Juan de Fuca ridge, an intermediate-rate spreading center, near the intersection with the Blanco transform fault. Their U–Th zircon crystallization ages ($29.3^{+4.8}_{-4.6}$ ka; 1σ standard error s.e.) overlap with the (U–Th)/He zircon eruption age (32.7 ± 1.6 ka) within uncertainty. Based on similar $^{238}U-^{230}Th$ disequilibria between southern Cleft dacite glass separates and young mid-ocean ridge basalt (MORB) erupted nearby, differentiation must have occurred rapidly, within ~10–20 ka at most. Ti-in-zircon thermometry indicates crystallization at 850–900 °C and pressures >70–150 MPa are calculated from H_2O solubility models. These time-temperature constraints translate into a magma cooling rate of $\sim 2 \times 10^{-2}$ °C/a. This rate is at least one order-of-magnitude faster than those calculated for zircon-bearing plutonic rocks from slow spreading ridges. Such short intervals for differentiation and cooling can only be resolved through uranium-series (^{238}U–^{230}Th) decay in young lavas, and are best explained by dissipating heat convectively at high crustal permeability.

1. Introduction

Large-volume liquid magma chambers once thought to dominate mid-ocean ridge environments are now known to be absent, even at fast-spreading ocean ridges (Sinton and Detrick, 1992). Recent models for axial ocean crust accretion that are consistent with this fact call for either down-and-out cumulate transport from a shallow magma lens ("gabbro glacier"; Coogan, 2007; Quick and Denlinger, 1993), or in-situ crystallization in a "sheeted-sill" complex comprising the entire lower crust (Coogan, 2007; Keleman and Aharonov, 1998; Kelemen et al., 1997). Geophysical models incorporating conductive and convective heat transport (Maclennan et al., 2005; Morton and Sleep, 1985) indicate that "sheeted-sill" accretion is only possible if pervasive hydrothermal convection efficiently dissipates heat from lower crustal magma bodies, whereas the gabbro-glacier model is largely independent of this constraint. Seismic imaging along the Juan de Fuca ridge (Canales et al., 2009) revealed that lower crustal melt sills exist at active spreading centers, although their longevity is unknown. Assessing long-term cooling rates for the lower ocean crust therefore remains crucial for testing the viability of existing models but such constraints are difficult to obtain. Pertinent petrological observations from active ridges and ophiolites are scarce and ambiguous because they have been interpreted to be consistent with either model (Coogan et al., 2007; VanTongeren et al., 2008). In this study, we examine newly discovered zircon-bearing evolved lavas that erupted near the ridge-transform intersection of the southernmost Juan de Fuca Ridge (Cleft segment) in order to quantify the rates of magmatic differentiation and high-temperature heat loss at an active spreading center through zircon thermochronology. We show that this approach has potential for providing new constraints on models of ocean crustal accretion.

2. Background

2.1. Zircon thermochronology in the oceanic environment

Zircon-bearing mid-ocean ridge (MOR) lavas have thus far gone undetected because lavas sufficiently evolved to crystallize zircon are exceedingly rare in these environments. Only ~1% of ~15,000 MOR

* Corresponding author.
E-mail address: axel@oro.ess.ucla.edu (A.K. Schmitt).

0012-821X/$ – see front matter © 2010 Elsevier B.V. All rights reserved.
doi:10.1016/j.epsl.2010.12.022

volcanic rock analyses in the PETDB database (http://www.petdb.org; Lehnert et al., 2000) have SiO_2 >57% which might be evolved enough to crystallize zircon. Despite being scarce in global databases, evolved lavas have erupted along several mid-ocean ridges, usually in specific tectonic settings, such as propagating ridge tips (Christie and Sinton, 1981; Fornari et al., 1983; Perfit et al., 1983), overlapping spreading centers (Bazin et al., 2001; Christie and Sinton, 1981; Sinton et al., 1983; Wanless et al., 2010), regions of ridge–hotspot interaction (Chadwick et al., 2005; Haase et al., 2005), and near ridge-transform intersections (Regelous et al., 1999; Sinton et al., 1983). They also occur more frequently at higher melt supply ridges (Rubin and Sinton, 2007). Intrusions of evolved magma forming plagiogranites have been known in dredge collections since the 1960s (e.g., Coleman and Peterman, 1975), and are common in ophiolites and in drilled sections of ocean crust (e.g., Dick et al., 2000; Rollinson, 2009). Hence, differentiated melts may be more common within the crust than erupted volumes suggest.

Zircon is an outstanding high-temperature (magmatic) geothermometer because of the sluggish diffusion of highly charged cations in its structure, and it is therefore well-behaved for U–Pb, (U–Th)/He, and Uranium-series (U-series) dating. Previously, this potential has only been harnessed for oceanic zircon from plutonic rocks generated in slow spreading ridge environments. U–Pb zircon ages of samples from the Mid-Atlantic Ridge (~13.5 Ma) indicate protracted crystallization durations over 0.090–0.235 Ma (Grimes et al., 2008; Lissenberg et al., 2009). Even longer crystallization intervals of up to 1.5–2.5 Ma have been reported for ~11–14 Ma old zircon in plutonic rocks from the Southwest Indian Ridge (Schwartz et al., 2005), translating into cooling rates of ~10^{-3}–10^{-4} °C/a for slow-spreading ridges (John et al., 2004). For the same location, (U–Th)/He zircon ages are in some cases up to 2.6 Ma younger than U–Pb crystallization ages, which suggest a subsequent pulse of hydrothermal heating (Schwartz et al., 2009).

The discovery of "volcanic" zircon in Juan de Fuca MOR lavas opens a new avenue for oceanic thermochronology because the young age of these lavas allows differentiation, crystallization, and eruption to be dated at high absolute temporal resolution through U-series methods, which is generally precluded by the older ages of zircon crystals in oceanic plutonic rocks (Grimes et al., 2008; Hellebrand et al., 2007; John et al., 2004; Lissenberg et al., 2009; Schwartz et al., 2005, 2009). This study is also the first zircon-thermochronology study of an intermediate-rate spreading center, with all of the prior work having been done at slow and ultraslow spreading ridges.

2.2. Geological setting of the southern Cleft segment of the Juan de Fuca Ridge

Lava samples ranging from typical MORB to dacite were collected in 2004 at the southern terminus of the Cleft segment of the Juan de Fuca Ridge, at its intersection with the Blanco Fracture Zone, using the remotely-operated-vehicle *Tiburon* of the Monterey Bay Aquarium Research Institute (Stakes et al., 2006). Dive 735 targeted two circular domes (~34 m high and ~200–500 m in diameter; Fig. 1) between 44°31′N and 44°29′N (Embley et al., 1991; Smith et al., 1994) where dacite glass had previously been sampled by wax rock core (Stakes et al., 2006). The southern Cleft domes sit in an area dominated by volcanic hummocks and hooked ridges that curve eastward towards the ridge-transform domain (Fig. 1), about 3 km south of the well-defined axial valley and approximately 1.5 to 2 km to the west of the extrapolation of the current ridge axis. To the south of this location, the axial ridge is believed to propagate past the Blanco Transform Zone into older ocean crust (~6.3 Ma) that was created at the Gorda Ridge (Embley and Wilson, 1992; Stakes et al., 2006). Seismic studies of the southern Juan de Fuca Ridge do not resolve an axial magma chamber south of 44°38′N, where the high silica lavas were recovered, whereas axial magma chamber reflectors occur at ~2 km below seafloor beneath most of the Cleft segment further north (Canales et al., 2006). This suggests that either only small pooled melt volumes exist in the crust, as a likely result of reduced melt supply in the region of the ridge-transform intersection, or that melt is only intermittently present at the end of the ridge segment.

The T735 domes lack significant sediment cover and samples have only thin (maximum ~1–2 mm) manganese coatings. The approximate off-axis distance and the half spreading rate of 28.5 ± 0.5 mm/year (Wilson, 1993) could be taken to imply that the domes are approximately 53–70 ka old had they formed directly on-axis, but it is not clear from the bathymetric features whether these lavas were erupted within or outside the ~2 km wide axial valley. Given their radiometrically determined eruption age (to be discussed in section 4.1), these lavas could be ~35 ka younger than the underlying crust that formed at the axial summit trough, but there is no evidence from U–Th model ages that would support this.

MORB lavas surrounding the domes are moderately differentiated ferrobasalts and FeTi basalts similar to those recovered along the ridge to the north (Stakes et al., 2006). In addition, large andesitic pillow lavas appear to have erupted from axis-bounding faults up 1 km from the axial summit trough to the north of the domes. Lavas comprising the domes themselves are high-silica andesites and dacites (SiO_2

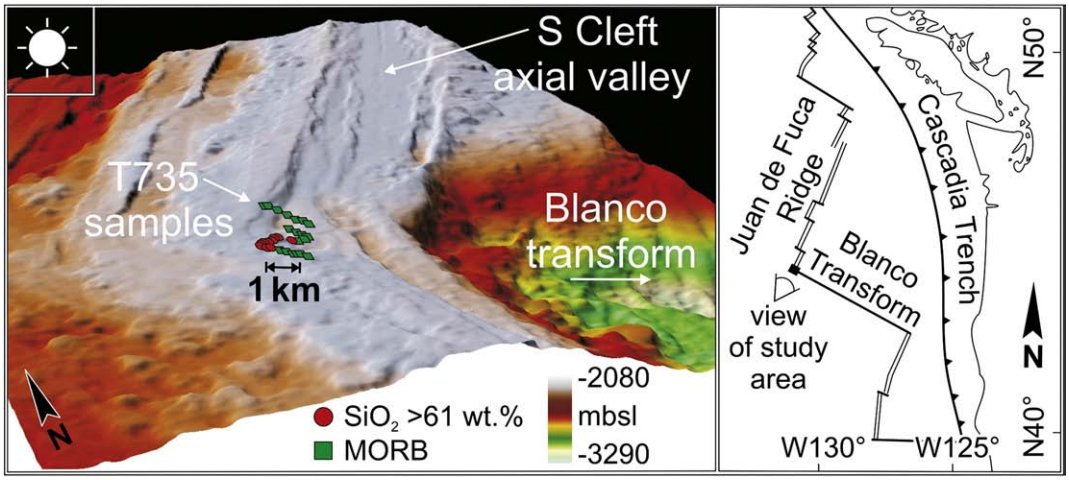

Fig. 1. Location of the study area (Juan de Fuca ridge and the Blanco transform fault intersection). Detailed bathymetric map shows the southernmost Cleft axial valley and its transition into hummocky curved ridges that hook around the deep transform fault zone (3× vertical exaggeration; mbsl = m below sea level). Track of dive T735 of the remotely operated vehicle Tiburon is represented by sampling locations where andesitic and dacitic samples (red circles) and typical MORB (green squares) were recovered.

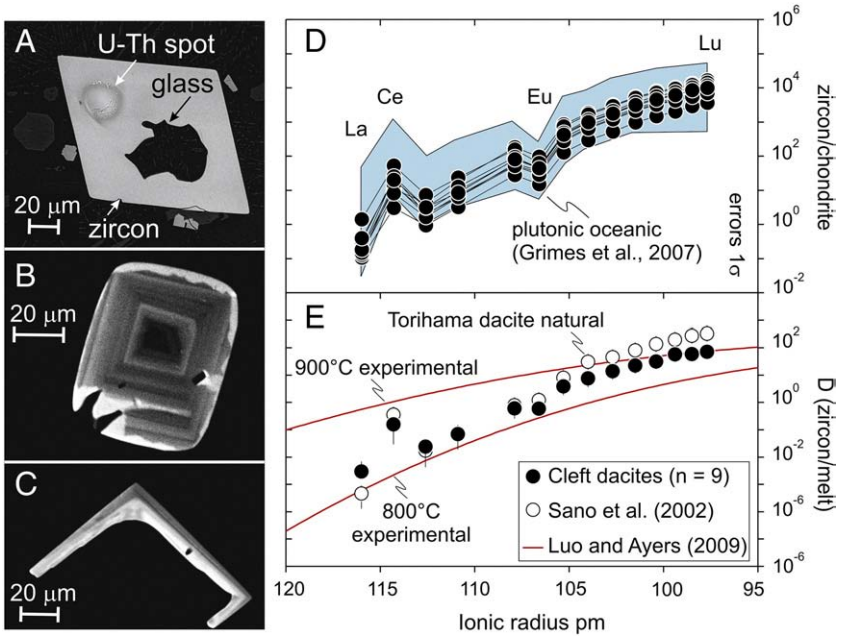

Fig. 2. Backscatter electron (BSE) and cathodoluminescence (CL) images of zircon crystals in southern Cleft dacite lavas. (A) Ion microprobe crater and glass inclusion in euhedral zircon (BSE). (B) Oscillatory zonation in CL-dark core truncated and overgrown by CL-bright rim, indicating intermittent resorption. (C) Skeletal zircon crystal. (D) Chondrite-normalized REE patterns for T735 zircon (solid circles) in comparison to field of plutonic oceanic zircon (Grimes et al., 2007). (E) Onuma plot of average zircon–melt partitioning D-values based on zircon compositions and whole-rock analyses (solid symbols; errors 1σ). D-values for southern Cleft lavas show a distinctively flatter pattern compared to Torihama dacite (Sano et al., 2002) (open symbols), but fall between experimental values for 800 and 900 °C (Luo and Ayers, 2009) (lines).

between 62.6 and 67.9 wt.%). Here, we collectively term them dacite for simplicity, acknowledging that matrix analyses straddle the compositional boundary between andesite and dacite. Glassy matrices are generally extremely vesicular (up to 10–15%, which is uncommon MOR volcanic rocks) and bubbles are elongated and range in size between ~1 mm and ~10 cm long.

Zircon crystals in these lavas are typically ~50–100 μm in length and mostly euhedral, but some exhibit irregular skeletal growth textures (Fig. 2). Oscillatory zones are sometimes embayed or truncated, and overgrown by euhedral rims (bright rims in Fig. 2B). This suggests crystallization near saturation where intermittent zircon resorption can occur. Pre-eruptive resorption is also indicated by rounded morphology of zircon crystals in high-silica andesites, possibly due to thermal and compositional effects of basaltic recharge and mixing with evolved magma. Notably, spongy zircon textures interpreted to result from metamorphic dissolution/reprecipitation reactions within the lower ocean crust and fluid overprinting (Schwartz et al., 2010), are absent.

3. Methods

U–Th zircon crystallization ages were initially determined in-situ on 35 crystal interiors from eight different southern Cleft lava samples, thereby avoiding potential contamination that can occur with pre-concentrated heavy mineral separates (c.f., Hellebrand et al., 2007). Approximately two to five zircon crystals were intersected per 27×46 mm area of thin-section (Fig. 2). U–Th isotopes in zircon were analyzed using the CAMECA ims 1270 ion microprobe at UCLA (Reid et al., 1997). Secular equilibrium standards AS3 (Paces and Miller, 1993) and 91500 (Wiedenbeck et al., 2004) repeatedly measured during the analysis period yielded a weighted average of (^{230}Th)/(^{238}U) = 1.012 ± 0.006 (1σ; MSWD = 0.68; n = 31). Selected crystals were also analyzed for trace element (including rare earth elements REE) and oxygen isotopic compositions by ion microprobe following established procedures (Monteleone et al., 2007; Trail et al., 2007).

After establishing that zircon crystals are entirely Late Pleistocene in age, we used crystal separates (obtained after crushing and heavy liquid separation) to determine U–Th zircon rim ages to a depth of ~5 μm by ion microprobe depth profiling (Table 1). This method preserves enough material to subsequently extract crystals from their mounting medium, and to determine individual (U–Th)/He eruption ages using facilities at the University of Kansas (Biswas et al., 2007). For this, crystals were wrapped in Pt foil, heated for 10 min at 1290 °C and reheated until >99% of the He was extracted from the crystal. After laser heating, crystals were unwrapped from the Pt foil and dissolved using double-step HF-HNO_3 and HCl pressure-vessel digestion procedures. U, Th, and Sm concentrations were determined by isotope dilution ICP-MS analysis. All ages were calculated using standard α-ejection corrections using morphometric analyses (Farley et al., 1996). The laboratory routinely analyzes zircon standards with independently determined ages, and we report averages for Fish Canon tuff zircon of 27.8 ± 0.8 Ma (RSD% = 7.5%, n = 285) and Durango zircon of 30.2 ± 1.1 Ma (RSD% = 6.8; n = 76). To correct for initial U-series disequilibrium, the D_{230} parameter (Farley et al., 2002) was determined from Th/U in zircon divided by the average Th/U of the glass matrix, and multiplied with 1.18 to account for the (^{230}Th)/(^{238}U) excess in the melt. D_{231} (defined analogous to D_{230} for ^{235}U–^{231}Pa decay) is estimated from the Pa/U zircon melt partitioning ratio of ~3 (Schmitt, 2007), and (^{231} Pa)/(^{235}U) melt excesses of ~2 from the literature (Goldstein et al., 1993). Uncertainties in these correction parameters are much smaller than analytical uncertainties of ~18% (1σ) estimated from the external reproducibility of the southern Cleft zircon analyses. Because the exact solution for the differential equations describing the production of He through decay of U and Th (Sm is reasonably neglected given the young age of our zircon crystals) can only be iteratively obtained, we calculated the disequilibrium-corrected (U–Th)/He zircon ages and uncertainties via Monte Carlo simulation using the MCHeCalc software (Schmitt et al., 2010) at 1,000,000 trials per each analysis.

U–Th–Ra isotopic analyses (Table 1) of glassy matrix separates of southern Cleft dacite and basalt lavas were conducted by thermal ionization mass spectrometry at University of Hawaii, using methods modified after Rubin et al. (2005). About 10 mg of each sample was hand-picked from 230 to 350 μm glass chips under a binocular

Table 1
U–Th compositions for T735 southern Cleft zircon and glassy matrix separates and (U–Th)/He zircon data.

Sample (depth in mbsl)	Latitude N	Longitude W	(^{238}U)/(^{232}Th)	(±)	(^{230}Th)/(^{232}Th)	(±)	U (ppm)	Th (ppm)	D_{230}	He (nmol/g)	mass (μg)	Ft	Uncorrected (U–Th)/He age (ka)	Corrected (U–Th)/He age (ka)	(+)	(−)
T735-G10 (2226) zircon 1	44.4994	−130.4732	6.37	0.13	2.61	0.30	163	87	0.21	0.0159	2.0	0.67	24.2	34.8	6.5	5.4
T735-G10 (2226) zircon 2	44.4994	−130.4732	6.57	0.11	2.28	0.36	123	69	0.22	0.0140	3.7	0.73	25.5	37.6	5.7	7.2
T735-G10 (2226) zircon 3	44.4994	−130.4732	6.96	0.14	2.53	0.41	130	77	0.24	0.0131	3.7	0.73	22.4	32.3	5.0	5.7
T735-G10 (2226) zircon 4	44.4994	−130.4732	6.67	0.14	2.44	0.33	169	98	0.23	0.0177	2.1	0.68	25.2	36.2	6.0	6.2
T735-G10 (2226) zircon 5	44.4994	−130.4732	6.53	0.12	2.75	0.40	137	78	0.23	0.0159	1.9	0.67	28.3	41.8	6.4	9.0
T735-G10 (2226) zircon 6	44.4994	−130.4732	6.78	0.11	2.16	0.29	97	55	0.23	0.0130	4.9	0.76	29.1	44.0	5.5	9.6
T735-G10 (2226) zircon 7	44.4994	−130.4732	6.70	0.12	2.79	0.33	130	64	0.20	0.0089	2.5	0.69	16.4	24.0	5.0	3.8
T735-G10 (2226) zircon 8	44.4994	−130.4732	6.82	0.12	2.36	0.33	125	57	0.18	0.0141	1.8	0.63	30.1	46.4	6.2	8.3
T735-G10 (2226) zircon 9	44.4994	−130.4732	7.04	0.17	2.58	0.75	44	20	0.18	0.0048	5.5	0.76	24.2	35.9	7.3	5.5
T735-G10 (2226) zircon 10	44.4994	−130.4732	7.25	0.12	3.06	0.52	174	87	0.20	0.0160	1.7	0.63	24.0	35.1	6.6	5.5
T735-G10 (2226) zircon 11	44.4994	−130.4732	7.99	0.15	1.95	0.97	91	47	0.21	0.0063	4.2	0.75	15.3	22.7	4.0	4.4
T735-G10 (2226) zircon 12	44.4994	−130.4732	6.99	0.11	2.59	0.37	147	73	0.20	0.0144	6.3	0.77	21.2	31.2	6.0	5.1
T735-G10 (2226) zircon 13	44.4994	−130.4732	8.34	0.17	4.21	1.34	73	34	0.19	0.0065	4.3	0.65	22.9	35.5	4.9	6.9
T735-G10 (2226) zircon 14	44.4994	−130.4732	8.32	0.16	3.14	0.91	66	29	0.18	0.0455	14	0.83	140	Excluded		
T735-G12 (2211) dacite	44.5000	−130.4737	1.191	0.003	1.343	0.008	1.190	3.032	–	–	–	–	–	–	–	–
T735-G18 (2206) high-silica andesite	44.5024	−130.4707	1.162	0.003	1.325	0.005	0.865	2.259	–	–	–	–	–	–	–	–
T178-G5 (2242) basaltic andesite	44.58	−130.4	1.184	0.003	1.387	0.007	0.476	1.220	–	–	–	–	–	–	–	–
T459-G10 (2153) FeTi basalt	44.65	−130.35	1.177	0.003	1.336	0.006	0.366	0.943	–	–	–	–	–	–	–	–
L1181WF-17 model MORB	44.66	−130.37	1.239	–	1.407	–	–	–	–	–	–	–	–	–	–	–

Parentheses denote activities; $D_{230} = [^{232}Th/^{238}U]_{zircon}/[^{232}Th/^{238}U]_{whole\text{-}rock}$; Ft = alpha particle ejection correction parameter.
Decay constants used: λ_{230}: $9.1577 \cdot 10^{-6}$ a^{-1}; λ_{232}: $4.9475 \cdot 10^{-11}$ a^{-1}; λ_{238}: 1.55125·10–10 a^{-1}; $\lambda_{226} = 4.332 \cdot 10^{-4}$ a^{-1}.
Zircon analyses by ion microprobe (activities from spot analyses), inductively coupled mass spectrometry (U, Th abundances from bulk crystal), and quadrupole mass spectrometry (He abundances from bulk crystal).
Error estimates from replicate analyses are 8% (1 s.d.) for Fish Canyon and Durango (U–Th)/He zircon ages and 18% (1 s.d.) for uncorrected T735-G10 zircon ages.
Glassy matrix analyses by thermal ionization mass spectrometry; U and Th abundance errors are 0.4 and 0.1% (relative), respectively.
(^{226}Ra)/(^{230}Th) of T178-G5 = 1.172 ± 0.014; T459-G10 = 0.996 ± 0.08.
Model MORB from Goldstein et al. (1992).

microscope to be free of alteration and basaltic inclusions. Samples were processed in a cleanroom environment using ultra-pure reagents with total procedural blanks of <2 pg for both Th and U. Samples were digested with an HF-HNO_3 mixture and subsequently split for Th and U isotope composition and concentration analyses on different solution fractions. Isotope dilution splits were spiked with ^{229}Th and ^{233}U tracers. Th and U were separated and purified from both sample splits by anion exchange chemistry. In order to accommodate the small sample sizes, ion exchange chemistry was conducted on 0.5 ml Teflon micro-columns rather than 4 ml Quartz glass columns. Analyses were conducted by single collector ion counter analysis on a Daly detector on a VG Sector 54 WARP, with one atomic mass unit abundance sensitivity of 20 ppb at mass 237 and baseline count rates of 0.1 to 0.3 cps. Accuracy and external reproducibility of ^{230}Th/^{232}Th and ^{234}U/^{238}U is better than 0.3% and 0.2%, based on repeat analyses of UCSC-A and CRM-112A during this project.

4. Results

4.1. Timing of dacite eruption, crystallization, and differentiation

The southern Cleft dacite average (U–Th)/He zircon age is 21.8 ± 1.2 ka (1 s.e.; $n=13$; Fig. 3), neglecting U-series disequilibria and omitting one grain with an unreasonably old age that had fractured during laser heating and from which U and Th was only incompletely recovered after He outgassing (Table 1). Without U-series disequilibria corrections, young (U–Th)/He zircon ages often significantly underestimate the eruption age because differential elemental partitioning between zircon and melt, and to lesser extent melt disequilibria, produce U-series disequilibria in zircon (Farley et al., 2002). Deficits in the long-lived intermediate daughter isotope ^{230}Th (half-life ~75.69 ka) delay He accumulation relative to equilibrium, whereas ^{231} Pa excesses (half-life ~32.76 ka) result in He that is unsupported by ^{235}U. After disequilibrium correction, the (U–Th)/He zircon age becomes 32.7 ± 1.6 ka (1 s.e.; goodness of fit Q = 0.23; $n=13$; Fig. 3). The corrected (U–Th)/He zircon age is indistinguishable from the U–Th zircon crystallization isochron age ($29.3^{+4.8}_{-4.6}$ ka; 1 s.e.; mean square of weighted deviates MSWD = 0.92; $n=49$; Fig. 4). We emphasize that these corrections, while significant, are mostly caused by the deficit in ^{230}Th (Farley et al., 2002), and that the other parameters (such as melt disequilibrium or ^{231}Pa excess) are of secondary importance.

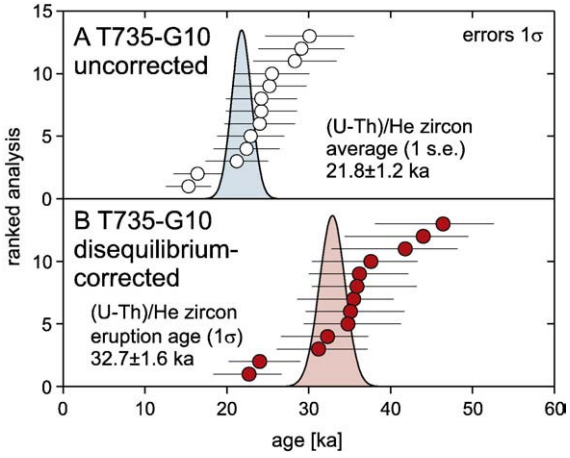

Fig. 3. (U–Th)/He zircon ages for southern Cleft dacites. (A) prior to correction for disequilibrium (1 s.e calculated as standard deviation divided by square-root of n); (B) disequilibrium-corrected (U–Th)/He ages with weighted average eruption age (1σ uncertainties).

Using the (U–Th)/He eruption age, we calculate initial melt (^{230}Th)/(^{232}Th)$_i$ = 1.396 ± 0.013 and 1.382 ± 0.009 for southern Cleft dacite samples T735-G12 and -G18, respectively. The ratios of southern Cleft MORB collected from the axial summit trough approximately 10 to 20 km to the north (Goldstein et al., 1992) are only slightly higher than these initial values (Table 1). In addition, axial lavas analyzed for this study have values similar to published data: basaltic andesite T178-G5 which has 17.2 ± 2.7% excess ^{226}Ra (attesting to its relative youth) has (^{230}Th)/(^{232}Th) = 1.387 ± 0.013, and other southern Cleft MORB with higher ^{226}Ra excesses (128 ± 6%) have average (^{230}Th)/(^{232}Th) = 1.407 ± 0.007 (Volpe and Goldstein, 1993) (Fig. 4B). The exact eruption ages for southern Cleft MORB lavas are unknown, but their (^{226}Ra)/(^{230}Th) overlaps with known zero-age northern Cleft MORB (137 ± 9% ^{226}Ra excess (Rubin et al., 2005)), consistent with a very recent eruption. The lower (^{226}Ra)/(^{230}Th) in nearby T178-G5 could indicate a slightly older eruption age.

Model U–Th differentiation durations were calculated using dacite (^{230}Th)/(^{232}Th)$_i$ at the time of eruption corresponding to the (U–Th)/He age of 32.7 ± 1.6 ka as the differentiated melt, and (^{230}Th)/(^{232}Th) = 1.407 for southern Cleft MORB as the parent (Allègre and Condomines, 1976). The rate at which (^{230}Th)/(^{232}Th) changes with time (t) depends on (^{238}U)/(^{232}Th) of the melt, and our calculations are for two limiting

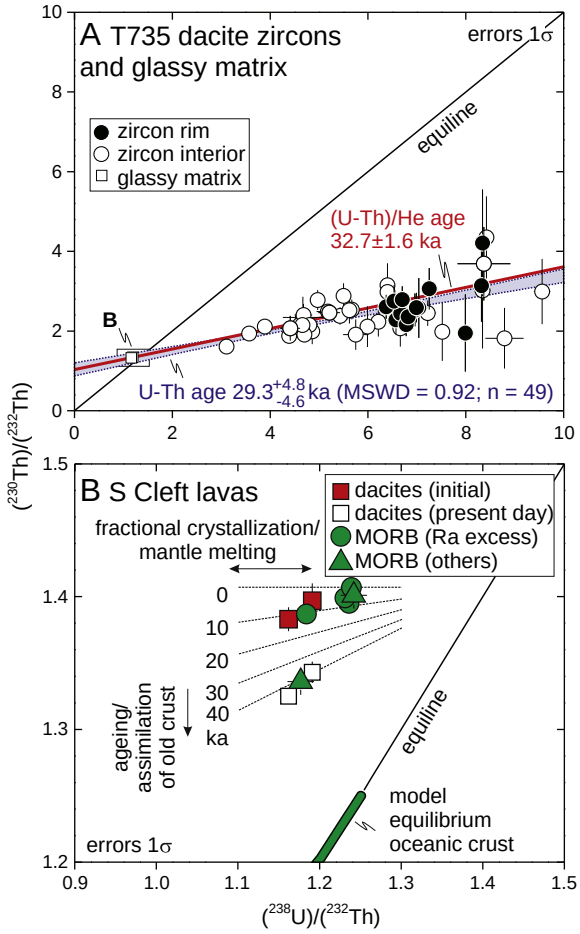

Fig. 4. U–Th activity diagram for southern Cleft dacite zircon and glassy matrix of host lavas. (A) Zircon rim (solid circles) and interiors (open circles) are indistinguishable, and yield an isochron (hatched area) that agrees closely with the (U–Th)/He eruption age (solid line). (B) present-day (open square) and initial (closed square) ratios for glassy matrix. Initial ratios are close to recent MORB (with ^{226}Ra disequilibrium; solid circle) from the axis of the southern Cleft (Goldstein et al., 1992; Volpe and Goldstein, 1993; this study). Other southern Cleft MORB samples where ^{226}Ra-excesses are absent or unknown are plotted for comparison (solid triangle). Arrows indicate general paths of mantle melting and fractional crystallization vs. ageing and assimilation of old crust (secular equilibrium MORB). Errors 1σ.

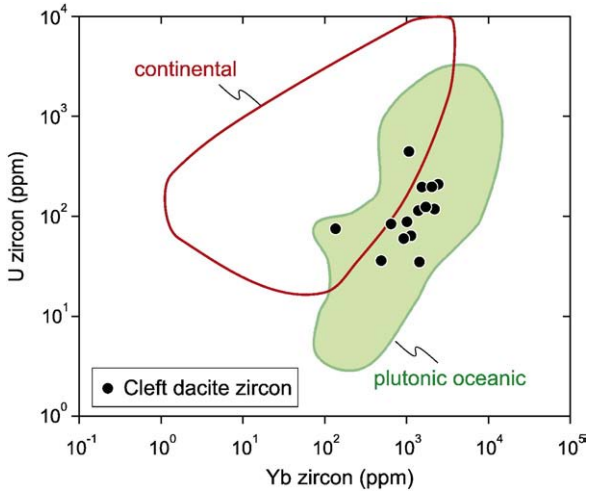

Fig. 5. U vs. Yb abundances of southern Cleft zircon. Note close overlap between the field of oceanic plutonic zircon and those from T735 dacite lavas. By contrast, zircon from continental crustal sources is displaced to higher U abundances (Grimes et al., 2010).

end-members in melt composition: (1) southern Cleft MORB, and (2) southern Cleft evolved magma. Mechanistically, scenario (1) would correspond to ageing of MORB magma (or young mafic crust), followed by rapid differentiation (or re-melting) to generate the evolved magma, whereas in scenario (2) the evolved magma would be generated early, and subsequently be stored at depth prior to eruption. Within these limits, the differentiation time-scales are 5.7 ± 6.3 ka and 11.8 ± 4.1 ka (scenario 1), and 7.3 ± 9.7 ka 17.7 ± 8.3 ka (scenario 2), for dacite T735-G12 and high-silica andesite-G18, respectively. Because values for both samples overlap within uncertainty, they are combined into two-sample average model differentiation ages of 10.0 ± 3.4 ka and 13.3 ± 6.3 ka for scenarios (1) and (2), respectively.

We stress that the previously discussed timescales are independent from the process by which dacites differentiated from the MORB reservoir because changes in ^{238}U–^{230}Th are only sensitive to radioactive decay in a closed system. Major element compositions of southern Cleft dacites are generally compatible with closed system fractional crystallization of MORB (e.g., Juster et al., 1989), but comparatively high incompatible trace element (Rb, Ba, U, and Th)

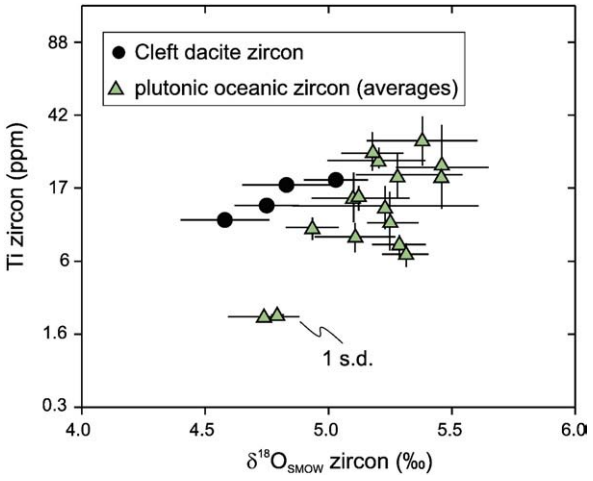

Fig. 6. Ti-in-zircon vs. $\delta^{18}O$ compositions for southern Cleft zircon. For comparison, oceanic plutonic zircon from plagiogranite, gabbro, and serpentinite samples from slow-spreading ridges are plotted (symbols and error bars represent averages and standard deviations; Grimes et al., 2010). The $\delta^{18}O$ values are slightly lower than those for plutonic zircon that are largely in equilibrium with differentiated MORB-derived melts, but the range of values overlaps.

and Cl enrichments in the dacites indicate a contribution of partial melts from amphibole-bearing altered ocean crust, whereby melting and assimilation could be facilitated by latent heat released from a crystallizing MORB magma lens (Wanless et al., 2010). The similar $(^{230}Th)/(^{232}Th)_i$ of southern Cleft dacites and MORB cannot be reconciled with a large contribution of partial melts derived from old (secular equilibrium) basaltic crust. If re-melting occurred, it would have involved young basaltic crust in disequilibrium. This is not unprecedented because remelting of young basaltic crust generating silicic melts has also been documented for a bimodal rock suite from Torfajokull-Veidivotn volcano in Iceland (Zellmer et al., 2008). The consanguinity between dacites and MORB is also supported by zircon oxygen isotopic compositions that are broadly consistent with fractional crystallization of parental MORB with a minor component of assimilated, hydrothermally altered crust. In this case, minor assimilation of pre-existing ocean crust would further reduce our model differentiation timescales.

It is also reasonable to assume that mantle melting parameters controlling MORB U/Th characteristics have not changed dramatically in this region over the past ~30 ka, and that modern southern Cleft MORB is a valid composition for late Pleistocene MORB. We argue that the lower U/Th of the dacites relative to modern MORB is unrelated to secular changes in MORB composition, but rather that apatite fractionation is the dominant factor controlling the lower dacite U/Th because of the low P_2O_5 abundances in the dacites and the strong correlation between U/Th and P_2O_5. Selecting a parent with lower $(^{230}Th)/(^{232}Th)$ (e.g., T178-G5), instead of the highest values measured in southern Cleft MORB we employed, would reduce differentiation timescales (to $\sim 0 \pm 4$ ka).

4.2. Conditions of zircon crystallization based on textures and trace elements

Rapid crystallization of zircon in southern Cleft dacites is indicated by skeletal zircon growth textures (Fig. 2C). Trace element abundances of southern Cleft zircon are close to those of oceanic plutonic zircon from slow and ultraslow spreading systems (Grimes et al., 2009). REE compositions and Ti abundances (Figs. 2, 5, 6; Supplementary Data) overlap the ranges observed in oceanic plutonic zircon (Grimes et al., 2009). We also determined zircon-melt partitioning coefficients (D-values) using abundances for hand-picked glassy matrix as representative of the melt. D-values are intermediate between experimental values at 800–900 °C (Luo and Ayers, 2009) and those that are considered typical for equilibrium partitioning (i.e., natural D-values for Torihama dacite zircon; Sano et al., 2002). This supports the textural evidence that southern Cleft zircon crystallized rapidly, and may not have fully achieved equilibrium, similar to the experimental conditions of Luo and Ayers (2009). Quantitatively, the indistinguishable U–Th rim and core crystallization ages (Fig. 4) limit zircon crystallization time-scales to within the analytical resolution of few 1000 years.

Average zircon crystallization temperatures of 905 ± 34 °C were calculated using Ti-in-zircon thermometry (Ferry and Watson, 2007; Watson and Harrison, 2005). We used silica activity $a(SiO_2) = 1$ (justified by the presence of quartz in mineral separates and granophyric clots). Titania activity $a(TiO_2) = 0.32 \pm 0.02$ was determined from coexisting Fe–Ti-oxides using an approach modified from Wark et al. (2007) who constrained $a(TiO_2)$ by combining oxygen fugacity and temperature constraints from Fe–Ti-oxide thermometry (Supplementary Data) with the internally consistent thermodynamic data set of Holland and Powell (1998). The lower pressure of zircon crystallization in mid-ocean ridge dacites (section 4.3) relative to the experimental calibration at 1 GPa (Ferry and Watson, 2007) would potentially lower Ti-in-zircon temperatures by 40–80 °C (Ferriss et al., 2008; Ferry and Watson, 2007). This would also bring Ti-in-zircon temperatures closer in line with the temperatures for zircon saturation (Watson and Harrison, 1983), which average 824 ± 15 °C

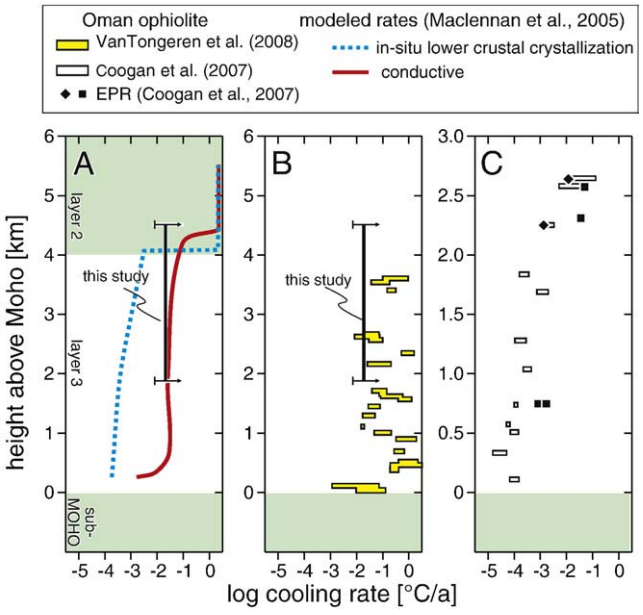

Fig. 7. Summary of petrological ocean crust cooling rates for fast spreading ridges. (A) Solid bar is for southern Cleft dacite cooling rates shows as the average (2×10^{-2} °C/a; solid bar) together with a lower limit (8×10^{-3} °C/a; left error bar at 95% confidence). Arrows to the right indicate the undefined upper limit for the cooling rate that results from the overlap between initial Th-isotopic compositions for the dacites and modern MORB within analytical uncertainties. Thermal model results for convection-dominated ("in-situ lower crustal", red, solid) and conductive cooling ("conductive", green, dotted) from Maclennan et al. (2004) plotted for comparison suggest that fast dacite cooling rates within layer 3 could only be achieved under conditions of convective heat transport. (B) Results of this study in comparison to cooling rates based on Ca-in-olivine diffusion from the Oman ophiolites (VanTongeren et al., 2008). (C) Ca-in-olivine diffusion cooling rates for a thinner section of the Oman ophiolite, plotted together with East Pacific Rise (EPR) dredge samples of known depth beneath the sheeted dike complex (Coogan et al., 2007) which are comparatively low for deep oceanic crustal layer 3. Note different scales in (C) relative to (A) and (B). Error bars for Ca-in-olivine diffusion do not reflect uncertainties in diffusion parameters.

(1 s.d.; $n=5$) for high-Si andesites, and 849 ± 19 °C (1 s.d.; $n=7$) for dacites. Fe–Ti oxide temperatures for dacite T735-G12 (~800–875 °C) overlap with zircon saturation and Ti-in-zircon thermometers, but show more variability, possibly due to re-equilibration during magma ascent and eruption.

Oxygen isotopic compositions of southern Cleft zircon fall near the lower range of those observed in oceanic plutonic zircon at similar Ti abundances (Fig. 6; Supplementary Data). This is compatible with the model of Grimes et al. (2010) for generating zircon-bearing evolved melts via MORB fractional crystallization, potentially coupled with minor assimilation of hydrothermally altered ocean crust.

4.3. Depth of dacite differentiation

Qualitatively, high H_2O-abundances in the southern Cleft dacite lavas are indicated by large and abundant vesicles. Water-saturated MORB crystallization experiments (Spulber and Rutherford, 1983) also imply high magmatic H_2O contents in order to suppress the solidus below the temperatures indicated by zircon thermometry. Plagioclase–liquid hygrometry (Lange et al., 2009) indicates initial melt H_2O contents between 3.2 wt.% (at 900 °C) and 4.2 wt.% (at 850 °C) for average groundmass plagioclase compositions in T735-G12 and -G16 (An = 35). These pre-eruptive H_2O estimates are largely pressure-insensitive, and translate into H_2O solubility pressures of ~70 and ~110 MPa (at 900 °C and 850 °C, respectively), calculated using the Moore et al. (1998) solubility model applied to southern Cleft dacites. Pressures could be higher if the melt was H_2O undersaturated, or CO_2 was present in the volatile phase. The absence of hornblende in southern Cleft dacites indicates an upper limit of ~150 MPa (Spulber and Rutherford, 1983) for the pressures at which the dacite magmas equilibrated. The lack of hornblende in the lavas alone does not rule out its former presence because it could have become resorbed during ascent and degassing. Whole-rock trace element patterns, however, lack any evidence for prior amphibole fractionation (Wanless et al., 2010), and we therefore assume that it was never stable under the conditions the dacite magmas equilibrated.

The ~70–150 MPa pressure window indicates that pre-eruptive dacite melt storage and zircon crystallization occurred near the top of, or well within lower ocean crust layer 3, at ~1.5 to 4.1 km depth below seafloor. Such depths are not unreasonable for generating evolved melts as indicated by the ubiquity of zircon-bearing plagiogranites in many lower crustal ophiolite sections (e.g., Amri et al., 1996; Mattinson and Hopson, 2008).

5. Discussion

5.1. Southern Cleft cooling rate estimates in comparison with other petrologic constraints

There is a ~200 °C minimum temperature difference between moderately fractionated MORB magma in the lower ocean crust (>1100 °C) and the eruption temperature of the dacites (900–850 °C). Using this difference, and the ~10–13 ka differentiation timescale, we calculate minimum cooling rates of ~$1.5–2.0\times10^{-2}$ °C/a (Fig. 7). These rates only apply to the high-temperature (magmatic) path of ocean crust cooling (cf. John et al., 2004; Schwartz et al., 2009 for estimates on low-T cooling rates of oceanic plutonic rocks from slow-spreading ridges). Our estimate for a(TiO_2) is at the lower global range for zircon-bearing melts which typically have a(TiO_2) >0.5, but lower values have been documented for natural rhyolites (Watson and Harrison, 2005). If we had overestimated the dacite magma temperature, for example by underestimating a(TiO_2), or if initial MORB temperatures were higher, these cooling rates would be even faster.

Cooling rates based on southern Cleft dacite zircon crystals are significantly faster than those derived from the ranges of Ti-in-zircon temperatures and U–Pb ages observed in gabbroic zircon fractions from the Vema Fracture Zone on the Mid-Atlantic Ridge (Lissenberg et al., 2009). Moreover, southern Cleft volcanic zircon appears to record a relatively simple crystallization history (i.e., the crystals lack evidence for protracted crystallization beyond the ±5 ka uncertainty of the U–Th isochron). This contrasts with protracted U–Pb ages for plutonic zircon from dredged and drilled samples of oceanic gabbro from slow and ultraslow spreading ridges (Grimes et al., 2008; Lissenberg et al., 2009; Schwartz et al., 2005). A possible explanation for this contrasting pattern is that cooling rates derived from MOR volcanic zircon reflect conditions experienced by an individual magma body, whereas plutonic rocks in slow and ultraslow spreading ridges may record multiple magmatic pulses occurring over more protracted time scales than at faster spreading ridges. In order to compare our data with previous petrologic and model results for intermediate- and fast spreading ridges, we plot cooling rate and depth estimates for a model crust with 6 km total thickness and a 2 km thick upper crust (layer 2), consistent with seismic data for the southern Cleft (Carbotte et al., 2008). Uncertainties are indicated by error bars corresponding to the lower cooling rate limit (8×10^{-3} °C/a) derived from propagating all U-series and eruption age uncertainties at 95% confidence. The data preclude reliable estimates for an upper cooling rate limit because dacite $(^{230}Th)/(^{232}Th)_i$ overlaps within uncertainties with modern MORB, which would yield an infinitively high rate (arrows in Fig. 7). Fig. 7 also summarizes existing petrological constraints for high-temperature cooling rates at intermediate to fast spreading centers. These are based on diffusive exchange thermometry (mainly Ca-in-olivine) for samples from the Oman ophiolite, and to lesser extent

plutonic rocks exposed along rifted sections of the East Pacific Rise (EPR) (Coogan et al., 2007; VanTongeren et al., 2008). Diffusive exchange thermometry has the advantage that cooling rates can be investigated along crustal transects exposed in ophiolite complexes, but the interpretation of such data is ambiguous because different case studies yielded variable results over small depth intervals that in some cases violate limiting constraints from geophysical models (VanTongeren et al., 2008). Specifically, Ca-in-olivine diffusion data from the Oman ophiolite in some cases appear to indicate decreasing cooling rates with depth consistent with conductive cooling (Coogan et al., 2007), yet in a different location of the same ophiolite the values span conditions estimated from models of convective cooling of the lower crust at uniform cooling rates (VanTongeren et al., 2008). Moreover, there are ambiguities with regard to Ca-in-olivine diffusion rates which increase absolute cooling rate uncertainties by two orders of magnitude (VanTongeren et al., 2008). For completeness, Fig. 7C also plots the few available Ca-in-olivine diffusion data from the EPR (Coogan et al., 2007). These EPR cooling rate estimates are highly variable, and in part their true depth within the lower crust is unknown, so they are of limited use for a comparison with our cooling rates. Recent plagioclase geospeedometric data from MOR basalts erupted at ultra-slow to intermediate spreading ridges, including the Juan de Fuca Coaxial segment, suggested that the vertical extent of melt lenses within the gabbroic layer is of the order of 1 m or less (Zellmer et al., 2010). This would favor rapid cooling rates, providing support for the sheeted sill model of oceanic crustal accretion.

5.2. Implications of southern Cleft dacite differentiation and cooling rates for ocean crustal accretion

The differentiation and cooling rates for dacitic magma generated in an MOR environment apply to the high temperature (magmatic) segment of the oceanic crustal cooling path. Oceanic crustal cooling rates in fast spreading centers have been modeled in several studies (e.g., Maclennan et al., 2004, 2005; Morton and Sleep, 1985), with contrasting predictions for cooling in the lower oceanic crust depending on the depth of magma intrusion. Because of the scarcity of petrologically constrained cooling rates, the comparison between our results to these model predictions is instructive for testing the viability of different models for oceanic crustal accretion. The limitations of such a comparison are discussed here.

In the framework of the gabbro-glacier model, rapid differentiation and cooling (which can be regarded as essentially equivalent) as constrained by the southern Cleft dacite lavas would only be possible if these melts were generated at the very top of ocean crust layer 3. In this location, the axial magma body is chilled against the cold upper crust, and fast cooling rates result from conductive heat dissipation advocated by the gabbro-glacier model (Fig. 7A). If, however, the higher-pressure barometric estimates are correct, then the equilibration of the southern Cleft dacite magma would have occurred within the lower crust well below the base of the sheeted-dike complex. In this scenario, our calculated cooling rates would be too fast to be consistent with a conductive cooling model (Fig. 7A). Instead, differentiation within the lower ocean crust would only be possible if most of the lower crust was convectively cooled via hydrothermal circulation as postulated for the sheeted-sill model (Boudier et al., 1996; Kelemen et al., 1997; Maclennan et al., 2005; VanTongeren et al., 2008).

Unfortunately, available barometric constraints are insufficient for precisely locating the depth of differentiation. There are, however, several reasons to assume that the upper depth estimate of ~1.5 km below seafloor is a minimum value. Because this estimate is based on a H_2O saturation model, higher pressures are possible if the melt was undersaturated. Moreover, the presence of dissolved CO_2 would also require higher pressures. In our calculations, we conservatively applied magmatic temperatures between 850 and 900 °C, whereas possible lower temperatures of 800 °C (well within the uncertainty of zircon-saturation and Fe–Ti-oxide geothermometers) would also translate into higher melt equilibrium pressure estimates.

Before extrapolating the results from the southern Cleft dacites to other intermediate and fast spreading centers, we re-emphasize that these lavas erupted in an atypical portion of the Juan de Fuca spreading center where it abuts cold and fractured ocean lithosphere at a ridge—transform intersection, so that cooling rates may differ from more normal areas of the global ridge system. Conductive cooling rates, however, should not differ much between axial magma bodies with old crust juxtaposed on one side, and those away from a ridge—transform intersection because horizontal diffusive heat dissipation would be minor relative to vertical heat loss for sill-shaped geometries.

For the case that the southern Cleft dacites erupted off-axis, they would only record cooling of a minor magma volume at the distal ends of the main locus of magma formation and differentiation beneath the axis. The curved geometry of the ridge segment studied here may also suggest propagation events or at least somewhat lower spreading rates than for the ridge segments away from the intersection to the north. For both scenarios, one might predict that the dacite domes were constructed on older, and potentially compositionally distinct MORB crust relative to that on the axis, and away from the ridge-transform intersection. The ferrobasalts and Fe–Ti basalts from the southern Cleft have major and trace element compositions that are similar to, but more evolved than, axial basalts erupted further north, suggesting that eruptions tapped magma that evolved in a similar fashion than MORB erupted along the central ridge axis, or that magma was supplied to the south via diking from the magmatically more robust region of the ridge to the north (Stakes et al., 2006). Hence, the geochemical data lack any indication that the crust-forming processes at the location of the southern Cleft dacite eruption differed significantly from those in a “normal” spreading environment.

To a first-order, we therefore consider the rapid cooling rates derived here to be broadly applicable to intermediate oceanic spreading centers. If more precise barometric constraints become available (e.g., from melt inclusion studies), it should be possible to refine the depth of magma differentiation and accumulation. This could eventually lead to a clearer distinction between differentiation in a high-level axial magma chamber, or a lower crustal intrusion, with significant implications for the viability of models for ocean crustal accretion.

6. Conclusions

The discovery of magmatic zircons in young volcanic rocks of the Juan de Fuca Ridge provides an unparalleled opportunity to examine the duration and character of magma differentiation at an active spreading center volcano. The southern Cleft dacite differentiation and cooling rates calculated here provide the first high-temporal-resolution constraints on these processes for an active spreading center. Zircon crystallization and eruption occurred rapidly within less than a few thousand years (essentially at the resolution of ^{230}Th–^{238}U-series dating). Estimates of the pressures of magma equilibration are consistent with a depth anywhere between the base of the sheeted-dike complex to moderate depths within the oceanic lower crust. Because the volatile-saturation based geobarometers that we have applied can only provide minimum estimates, rapid differentiation and cooling in the lower crust appears more likely.

Acknowledgements

Debra S. Stakes, the crew of the R/V Western Flyer, and the pilots of the ROV Tiburon are acknowledged for support during the sampling cruise. Janet C. Harvey is thanked for processing bathymetry data. We

thank reviewers Joshua Schwartz and Michel Condomines, as well as editor Richard Carlson. The ion microprobe facility at UCLA is partly supported by a grant from the Instrumentation and Facilities Program, Division of Earth Sciences, National Science Foundation. MRP, KHR, MCS and LAC were supported by grants from the Ocean Sciences Division of the NSF (OCE-0221541, Perfit; OCE-0933884, Rubin). WIR publishes with the permission of the US Geologic Survey.

Appendix A. Supplementary data

Supplementary data to this article can be found online at doi:10.1016/j.epsl.2010.12.022.

References

Allègre, C.J., Condomines, M., 1976. Fine chronology of volcanic processes using ^{238}U–^{232}Th systematics. Earth Planet. Sci. Lett. 28, 395–406.
Amri, I., Benoit, M., Ceuleneer, G., 1996. Tectonic setting for the genesis of oceanic plagiogranites: evidence from a paleo-spreading structure in the Oman ophiolite. Earth Planet. Sci. Lett. 139(1–2), 177–194.
Bazin, S., Harding, A.J., Kent, G.M., Orcutt, J.A., Tong, C.H., Pye, J.W., Singh, S.C., Barton, P.J., Sinha, M.C., White, R.S., Hobbs, R.W., Van Avendonk, H.J.A., 2001. Three-dimensional shallow crustal emplacement at the 9 degrees 03'N overlapping spreading center on the East Pacific Rise: correlations between magnetization and tomographic images. J. Geophys. Res. Solid Earth 106 (B8), 16101–16117.
Biswas, S., Coutand, I., Grujic, D., Hager, C., Stockli, D., Grasemann, B., 2007. Exhumation and uplift of the Shillong plateau and its influence on the eastern Himalayas: new constraints from apatite and zircon (U–Th-[Sm])/He and apatite fission track analyses. Tectonics 26 (6), 1–22. doi:10.1029/2007TC002125 (TC6013).
Boudier, F., Nicolas, A., Ildefonse, B., 1996. Magma chambers in the Oman ophiolite: fed from the top and the bottom. Earth Planet. Sci. Lett. 144 (1–2), 239–250.
Canales, J.P., Nedimovic, M.R., Kent, G.M., Carbotte, S.M., Detrick, R.S., 2009. Seismic reflection images of a near-axis melt sill within the lower crust at the Juan de Fuca ridge. Nature 460 (7251), 89–100.
Canales, J.P., Singh, S.C., Detrick, R.S., Carbotte, S.M., Harding, A., Kent, G.M., Diebold, J.B., Babcock, J., Nedimovic, M.R., 2006. Seismic evidence for variations in axial magma chamber properties along the southern Juan de Fuca Ridge. Earth Planet. Sci. Lett. 246 (3–4), 353–366.
Carbotte, S.M., Nedimovic, M.R., Canales, J.P., Kent, G.M., Harding, A.J., Marjanovic, M., 2008. Variable crustal structure along the Juan de Fuca Ridge: influence of on-axis hot spots and absolute plate motions. Geochem. Geophys. Geosyst. 9 (Q08001), 1–23. doi:10.1029/2007GC001922.
Chadwick, J., Perfit, M., Ridley, I., Jonasson, I., Kamenov, G., Chadwick, W., Embley, R., le Roux, P., Smith, M., 2005. Magmatic effects of the Cobb hot spot on the Juan de Fuca Ridge. J. Geophys. Res. 110 (B03101), 1–16. doi:10.1029/2003JB002767.
Christie, D.M., Sinton, J.M., 1981. Evolution of abyssal lavas along propagating segments of the Galapagos spreading center. Earth Planet. Sci. Lett. 56, 321–335.
Coleman, R.G., Peterman, Z.E., 1975. Oceanic plagiogranite. J. Geophys. Res. 80, 1099–1108.
Coogan, L.A., 2007. The Lower Oceanic Crust. In: Heinrich, D.H., Karl, K.T. (Eds.), Treatise on Geochemistry. Pergamon, Oxford, pp. 1–45.
Coogan, L.A., Jenkin, G.R.T., Wilson, R.N., 2007. Contrasting cooling rates in the lower oceanic crust at fast- and slow-spreading ridges revealed by geospeedometry. J. Petrol. 48 (11), 2211–2231.
Dick, H.J.B., Natland, J.H., Alt, J.C., Bach, W., Bideau, D., Gee, J.S., Haggas, S., Hertogen, J.G. H., Hirth, G., Holm, P.M., Ildefonse, B., Iturrino, G.J., John, B.E., Kelley, D.S., Kikawa, E., Kingdon, A., LeRoux, P.J., Maeda, J., Meyer, P.S., Miller, D.J., Naslund, H.R., Niu, Y.L., Robinson, P.T., Snow, J., Stephen, R.A., Trimby, P.W., Worm, H.U., Yoshinobu, A., 2000. A long in situ section of the lower ocean crust: results of ODP Leg 176 drilling at the Southwest Indian Ridge. Earth Planet. Sci. Lett. 179 (1), 31–51.
Embley, R.W., Chadwick, W., Perfit, M.R., Baker, E.T., 1991. Geology of the northern Cleft Segment, Juan de Fuca Ridge; Recent lava flows, sea-floor spreading, and the formation of megaplumes. Geology 19 (8), 769–775.
Embley, R.W., Wilson, D.S., 1992. Morphology of the Blanco Transform-Fault Zone-Ne Pacific—implications for its tectonic evolution. Mar. Geophys. Res. 14 (1), 25–45.
Farley K.A., Wolf R.A., Silver L.T., 1996. The effects of long alpha-stopping distances on (U-Th)/He ages. Geochim. Cosmochim. Acta 60 (21), 4223–4229.
Farley, K.A., Kohn, B.P., Pillans, B., 2002. The effects of secular disequilibrium on (U–Th)/He systematics and dating of Quaternary volcanic zircon and apatite. Earth Planet. Sci. Lett. 201 (1), 117–125.
Ferriss, E.D.A., Essene, E.J., Becker, U., 2008. Computational study of the effect of pressure on the Ti-in-zircon geothermometer. Eur. J. Mineralog. 20 (5), 745–755.
Ferry, J.M., Watson, E.B., 2007. New thermodynamic models and revised calibrations for the Ti-in-zircon and Zr-in-rutile thermometers. Contrib. Mineralog. Petrol. 154, 429–437.
Fornari, D.J., Perfit, M.R., Malahoff, A., Embley, R., 1983. Geochemical studies of abyssal lavas recovered by Dsrv Alvin from Eastern Galapagos Rift, Inca Transform, and Ecuador Rift .1. Major element variations in natural glasses and spacial distribution of lavas. J. Geophys. Res. 88 (NB12), 519–529.
Goldstein, S.J., Murrell, M.T., Janecky, D.R., Delaney, J.R., Clague, D.A., 1992. Geochronology and petrogenesis of MORB from the Juan-De-Fuca and Gorda Ridges by 238U–230Th disequilibrium. Earth Planet. Sci. Lett. 109 (1–2), 255–272.
Goldstein, S.J., Murrell, M.T., Williams, R.W., 1993. ^{231}Pa and ^{230}Th chronology of midocean ridge basalts. Earth Planet. Sci. Lett. 115 (1–4), 151–159.
Grimes, C., Ushikubo, T., John, B.E., Valley, J.W., 2010. Uniformly mantle-like δ^{18}O in zircons from oceanic plagiogranites and gabbros. Contrib. Mineralog. Petrol. doi:10.1007/s00410-010-0519-x.
Grimes, C.B., John, B.E., Cheadle, M.J., Mazdab, F.K., Wooden, J.L., Swapp, S., Schwartz, J.J., 2009. On the occurrence, trace element geochemistry, and crystallization history of zircon from in situ ocean lithosphere. Contrib. Mineralog. Petrol. 158 (6), 757–783.
Grimes, C.B., John, B.E., Cheadle, M.J., Wooden, J.L., 2008. Protracted construction of gabbroic crust at a slow spreading ridge: constraints from ^{206}Pb/^{238}U zircon ages from Atlantis Massif and IODP Hole U1309D (30 degrees N, MAR). Geochem. Geophys. Geosyst. 9 (Q08012), 1–24. doi:10.1029/2008GC002063.
Grimes, C.B., John, B.E., Kelemen, P.B., Mazdab, F.K., Wooden, J.L., Cheadle, M.J., Hanghoj, K., Schwartz, J.J., 2007. Trace element chemistry of zircons from oceanic crust; a method for distinguishing detrital zircon provenance. Geology 35 (7), 643–646.
Haase, K.M., Stroncik, N.A., Hekinian, R., Stoffers, P., 2005. Nb-depleted andesites from the Pacific-Antarctic Rise as analogs for early continental crust. Geology 33 (12), 921–924.
Hellebrand, E., Möller, A., Whitehouse, M., Cannat, M., 2007. Formation of oceanic zircons. Geochim. Cosmochim. Acta 71 (15), A391-A391.
Holland, T.J.B., Powell, R., 1998. An internally consistent thermodynamic data set for phases of petrological interest. J. Metamorph. Geol. 16 (3), 309–343.
John, B.E., Foster, D.A., Murphy, J.M., Cheadle, M.J., Baines, A.G., Fanning, C.M., Copeland, P., 2004. Determining the cooling history of in situ lower oceanic crust—Atlantis Bank, SW Indian Ridge. Earth Planet. Sci. Lett. 222 (1), 145–160.
Juster, T.C., Grove, T.L., Perfit, M.R., 1989. Experimental constraints on the generation of Fe–Ti basalts, andesites, and rhyodacites at the Galapagos spreading center, 85 degrees W and 95 degrees W. J. Geophys. Res. 94 (B7), 9251–9274.
Kelemen, P.B., Koga, K., Shimizu, N., 1997. Geochemistry of gabbro sills in the crust–mantle transition zone of the Oman ophiolite: implications for the origin of the oceanic lower crust. Earth Planet. Sci. Lett. 146 (3–4), 475–488.
Keleman, P., Aharonov, E., 1998. Periodic formation of magma fractures and generation of layered gabbros in the lower crust beneath oceanic spreading ridges. In: Buck, W.R., Delaney, P.T., Karson, J.A., Lagabrielle, Y. (Eds.), Faulting and Magmatism at Mid-Ocean Ridges: Geophysical Monograph Series American Geophysical Union, Washington, vol. 106, pp. 267–289.
Lange, R.A., Frey, H.M., Hector, J., 2009. A thermodynamic model for the plagioclase-liquid hygrometer/thermometer. Am. Mineralog. 94(4), 494–506.
Lehnert, K., Su, Y., Langmuir, C., Sarbas, B., Nohl, U., 2000. A global geochemical database structure for rocks. Geochem. Geophys. Geosyst. 1 (5), 1–14. doi:10.1029/1999GC000026 (1012).
Lissenberg, C.J., Rioux, M., Shimizu, N., Bowring, S.A., Mevel, C., 2009. Zircon dating of oceanic crustal accretion. Science 323 (5917), 1048–1050.
Luo, Y., Ayers, J.C., 2009. Experimental measurements of zircon/melt trace-element partition coefficients. Geochim. Cosmochim. Acta 73 (12), 3656–3679.
Maclennan, J., Hulme, T., Singh, S.C., 2004. Thermal models of oceanic crustal accretion: linking geophysical, geological and petrological observations. Geochem. Geophys. Geosyst. 5 (2), 1–32. doi:10.1029/2003GC000605 (Q02F25).
Maclennan, J., Hulme, T., Singh, S.C., 2005. Cooling of the lower oceanic crust. Geology 33 (5), 357–360.
Mattinson, J.M., Hopson, C.A., 2008. New high-precision CA-TIMS U/Pb zircon plateau ages for the Point Sal and San Simeon ophiolite remnants, California Coast Ranges. Spec. Pap. Geol. Soc. Am. 438, 103–112.
Monteleone, B.D., Baldwin, S.L., Webb, L.E., Fitzgerald, P.G., Grove, M., Schmitt, A.K., 2007. Late Miocene–Pliocene eclogite facies metamorphism, D'Entrecasteaux Islands, SE Papua New Guinea. J. Metamorph. Geol. 25 (2), 245–265.
Moore, G., Vennemann, T., Carmichael, I.S.E., 1998. An empirical model for the solubility of H2O in magmas to 3 kilobars. Am. Mineralog. 83(1–2), 36–42.
Morton, J.L., Sleep, N.H., 1985. A mid-ocean ridge thermal-model—constraints on the volume of axial hydrothermal heat-flux. J. Geophys. Res. Solid Earth Planet. 90 (NB13), 1345–1353.
Paces, J.B., Miller Jr., J.D., 1993. Precise U–Pb ages of Duluth Complex and related mafic intrusions, northeastern Minnesota; geochronological insights to physical, petrogenetic, paleomagnetic, and tectonomagnetic processes associated with the 1.1 Ga Midcontinent Rift System. J. Geophys. Res. B Solid Earth Planet. 98 (8), 13, 997–14, 013.
Perfit, M.R., Fornari, D.J., Malahoff, A., Embley, R.W., 1983. Geochemical studies of abyssal lavas recovered by DSRV Alvin from Eastern Galapagos Rift, Inca Transform, and Ecuador Rift. 3. Trace-element abundances and petrogenesis. J. Geophys. Res. 88 (NB12), 551–572.
Quick, J.E., Denlinger, R.P., 1993. Ductile deformation and the origin of layered gabbro in ophiolites. J. Geophys. Res. Solid Earth 98 (8), 14015–14027.
Regelous, M., Niu, Y.L., Wendt, J.I., Batiza, R., Greig, A., Collerson, K.D., 1999. Variations in the geochemistry of magmatism on the East Pacific Rise at 10 degrees 30'N since 800 ka. Earth Planet. Sci. Lett. 168 (1–2), 45–63.
Reid, M.R., Coath, C.D., Harrison, T.M., McKeegan, K.D., 1997. Prolonged residence times for the youngest rhyolites associated with Long Valley Caldera; ^{230}Th–^{238}U ion microprobe dating of young zircons. Earth Planet. Sci. Lett. 150 (1–2), 27–39.
Rollinson, H., 2009. New models for the genesis of plagiogranites in the Oman ophiolite. Lithos 112, 603–614.
Rubin, K.H., van der Zander, I., Smith, M.C., Bergmanis, E.C., 2005. Minimum speed limit for ocean ridge magmatism from ^{210}Pb–^{226}Ra–^{230}Th disequilibria. Nature 437 (7058), 534–538.
Rubin, K.H., Sinton, J.M., 2007. Inferences on mid-ocean ridge thermal and magmatic structure from MORB compositions. Earth Planet. Sci. Lett. 260, 257–276.

Sano, Y., Terada, K., Fukuoka, T., 2002. High mass resolution ion microprobe analysis of rare earth elements in silicate glass, apatite and zircon: lack of matrix dependency. Chem. Geol. 184 (3–4), 217–230.
Schmitt, A.K., 2007. Ion microprobe analysis of (^{231}Pa)/(^{235}U) and an appraisal of protactinium partitioning in igneous zircon. Am. Mineralog. 92, 691–694.
Schmitt, A.K., Stockli, D.F., Niedermann, S., Lovera, O.M., Hausback, B.P., 2010. Eruption ages of Las Tres Vírgenes volcano (Baja California): a tale of two helium isotopes. Quat. Geochronol. 5, 503–511.
Schwartz, J.J., John, B.E., Cheadle, M.J., Miranda, E.A., Grimes, C.B., Wooden, J.L., Dick, H.J.B., 2005. Dating the growth of oceanic crust at a slow-spreading ridge. Science 310 (5748), 654–657.
Schwartz, J.J., John, B.E., Cheadle, M.J., Reiners, P.W., Baines, A.G., 2009. Cooling history of Atlantis Bank oceanic core complex: evidence for hydrothermal activity 2.6 Ma off axis. Geochem. Geophys. Geosyst. 10 (Q08020), 1–28. doi:10.1029/2009GC002466.
Schwartz, J.J., John, B.E., Cheadle, M.J., Wooden, J.L., Mazdab, F., Swapp, S., Grimes, C.B., 2010. Dissolution–reprecipitation of igneous zircon in mid-ocean ridge gabbro, Atlantis Bank, Southwest Indian Ridge. Chem. Geol. 274 (1–2), 68–81.
Sinton, J.M., Wilson, D.S., Christie, D.M., Hey, R.N., Delaney, J.R., 1983. Petrologic consequences of rift propagation on oceanic spreading ridges. Earth Planet. Sci. Lett. 62 (2), 193–207.
Sinton, J.M., Detrick, R.S., 1992. Mid-ocean ridge magma chambers. J. Geophys. Res. 97 (B1), 197–216.
Smith, M.C., Perfit, M.R., Jonasson, I.R., 1994. Petrology and geochemistry of basalts from the southern Juan de Fuca Ridge; controls on the spatial and temporal evolution of mid-ocean ridge basalt. J. Geophys. Res. 99 (B3), 4787–4812.
Spulber, S.D., Rutherford, M.J., 1983. The origin of rhyolite and plagiogranite in oceanic-crust—an experimental-study. J. Petrol. 24 (1), 1–25.
Stakes, D.S., Perfit, M.R., Tivey, M.A., Caress, D.W., Ramirez, T.M., Maher, N., 2006. The Cleft revealed; geologic, magnetic, and morphologic evidence for construction of upper oceanic crust along the southern Juan de Fuca Ridge. Geochem. Geophys. Geosyst. 7 (4), 1–32. doi:10.1029/2005GC001038 (Q04003).
Trail, D., Mojzsis, S.J., Harrison, T.M., Schmitt, A.K., Watson, E.B., Young, E.D., 2007. Constraints on Hadean zircon protoliths from oxygen isotopes, Ti-thermometry, and rare earth elements. Geochem. Geophys. Geosyst. 8 (Q06014), 1–22. doi:10.1029/2006GC001449.
VanTongeren, J.A., Kelemen, P.B., Hanghoj, K., 2008. Cooling rates in the lower crust of the Oman ophiolite: Ca in olivine, revisited. Earth Planet. Sci. Lett. 267 (1–2), 69–82.
Volpe, A.M., Goldstein, S.J., 1993. Ra-226 Th-230 disequilibrium in axial and off-axis midocean ridge basalts. Geochim. Cosmochim. Acta 57 (6), 1233–1241.
Wanless, D., Perfit, M.R., Ridley, I.W., Klein, E., 2010. Dacite petrogenesis on mid-ocean ridges: evidence for oceanic crustal melting and assimilation. J. Petrol. 51 (12), 2377–2410.
Wark, D.A., Hildreth, W., Spear, F.S., Cherniak, D.J., Watson, E.B., 2007. Pre-eruption recharge of the Bishop magma system. Geology 35 (3), 235–238.
Watson, E.B., Harrison, T.M., 1983. Zircon saturation revisited; temperature and composition effects in a variety of crustal magma types. Earth Planet. Sci. Lett. 64 (2), 295–304.
Watson, E.B., Harrison, T.M., 2005. Zircon thermometer reveals minimum melting conditions on earliest Earth. Science 308 (5723), 841–844.
Wiedenbeck, M., Hanchar, J.M., Peck, W.H., Sylvester, P., Valley, J., Whitehouse, M., Kronz, A., Morishita, Y., Nasdala, L., Fiebig, J., Franchi, I., Girard, J.P., Greenwood, R.C., Hinton, R., Kita, N., Mason, P.R.D., Norman, M., Ogasawara, M., Piccoli, P.M., Rhede, D., Satoh, H., Schulz-Dobrick, B., Skar, O., Spicuzza, M.J., Terada, K., Tindle, A., Togashi, S., Vennemann, T., Xie, Q., Zheng, Y.F., 2004. Further characterisation of the 91500 zircon crystal. Geostand. Geoanal. Res. 28 (1), 9–39.
Wilson, D.S., 1993. Confidence intervals for motion and deformation of the Juan de Fuca Plate. J. Geophys. Res. 98 (B9), 16, 053–16, 071.
Zellmer, G.F., Rubin, K.H., Gronvold, K., Jurado-Chichay, Z., 2008. On the recent bimodal magmatic processes and their rates in the Torfajokull-Veidivotn area, Iceland. Earth Planet. Sci. Lett. 269 (3–4), 387–397.
Zellmer, G.F., Rubin, K.H., Dulski, P., Iizuka, Y., Goldstein, S.L., Perfit, M.R., 2010. Crystal growth during dike injection of MOR basaltic melts: evidence from preservation of local Sr disequilibria in plagioclase. Contrib. Mineralog. Petrol. doi:10.1007/s00410-010-0518-y.